This is a preprint draft. The published article can be found at: https://doi.org/10.12989/scs.2021.41.5.625

Please cite this paper as:
Zhou, H., Li, S., Zhang, C., **Naser M.Z.** (2021). "Modeling fire performance of externally prestressed steel–concrete composite beams." *Steel and Composite Structures.* https://doi.org/10.12989/scs.2021.41.5.625

Modeling Fire Performance of Externally Prestressed steel–concrete Composite Beams

Huanting Zhou[1], Shaoyuan Li[1], Chao Zhang[2], M.Z. Naser[3,*]

[1] *School of Civil Engineering and Architecture, Wuhan University of Technology, Wuhan 430072, China*
[2] *College of Civil Engineering, Tongji University, Shanghai 200092,China*
[3,*] *Glenn Department of Civil Engineering, Clemson University, South Carolina, US, E-mail: mznaser@clemson.edu, m@mznaser.com, Website: www.mznaser.com*

Abstract This paper examines the fire performance of uninsulated and uncoated restrained steel-concrete composite beams supplemented with externally prestressed strands through advanced numerical simulation. In this work, a sequentially coupled thermo-mechanical analysis is carried out using ABAQUS. This analysis utilizes a highly nonlinear three-dimensional finite element (FE) model that is specifically developed and validated using full-sized specimens tested in a companion fire testing program. The developed FE model accounts for nonlinearities arising from geometric features and material properties, as well as complexities resulting from prestressing systems, fire conditions, and mechanical loadings. Four factors are of interest to this work including effect of restraints (axial vs. rotational), degree of stiffness of restraints, the configuration of external prestressed tendons, and magnitude of applied loading. The outcome of this analysis demonstrates how the prestressing force in the external tendons is primarily governed by the magnitude of applied loading and experienced temperature level. Interestingly, these results also show that the stiffness of axial restraints has a minor influence on the failure of restrained and prestressed steel-concrete composite beams. When the axial restraint ratio does not exceed 0.5, the critical deflection of the composite beam is lower than that of the composite beam with a restraint ratio of 1.0.

Keywords: Fire resistance; Prestressed composite steel-concrete beams; Finite element analysis; Axial and rotational restraints.

1.0 Introduction

Externally prestressed steel-concrete composite beams (PCBs) were initially developed in the late 1950s (Hoadley, 1963; Szilard, 1959). These novel composite structural elements comprise of four main components. A typical PCB consists of a *steel beam* (often in the form of an I-shape) that is prestressed via *external tendons* while being connected to a *concrete slab* through *shear studs*. The novelty in PCBs, as opposed to traditional composite beams, arises from incorporating externally prestressed steel tendons (strands). These tendons change the mechanics of load transfer in PCBs and allow such elements to have a far greater flexural strength; thus, spanning much larger spans while undergoing minimal deflections as compared to their conventional counterparts. As Chen (2005) addressed in the literature, PCBs are widely used in conference halls, ballrooms etc.

As it is common in the field of structural engineering, the behavior and performance of PCBs were heavily investigated (both experimentally and theoretically) at ambient working conditions over the past two decades (Chen, 2005; Chen et al., 2009; Dall'Asta et al., 2002; Deretic-Stojanovic and Kostic, 2017; Kim and Lee, 2011; Lee et al., 2015; Lorenc and Kubica, 2006; Ng and Tan, 2006a, 2006b; Ren et al., 2018; Zona et al., 2009). For instance, Chen and colleagues explored different configurations of PCBs. In such a study, Chen et al. (2009) tested continuous PCBs and noted significant improvements in their structural behavior. Such improvements were mainly attributed to the ability of PCBs to effectively redistribute forces between hogging and sagging regions through prestressed

tendons (Chen et al., 2009). In a companion work, Chen et al. (2005) experimentally explored the cracking behavior and moment resistance of PCBs in sagging and hogging regions. These researchers reported that while using externally prestressed tendons effectively improved PCBs' moment capacity in the positive (sagging) region, the benefits of these tendons seem to only slightly improve the ultimate hogging moment capacity of the same PCBs.

In a similar manner, Lorenc and Kubica (2006) investigated the behavior of PCBs under positive bending by testing large-sized specimens. In their experiments, six simply supported beams with different tendon arrangements, varying between straight, draped, and no tendons were tested to failure. These tests confirmed that the configuration of prestressed tendons does not seem to affect PCBs' structural response (given that the examined configuration maintained the same eccentricity of tendons). Other researchers also carried out tests on PCBs. For example, Ng and Tan (2006a) tested nine simply supported PCBs and noted that the span-to-depth ratio in PCBs had a minor effect on the flexural behavior of PCBs. Kim and Lee (2011) experimentally investigated the flexural behavior of PCBs with corrugated webs and found that these prestressed beams had superior flexural strength and stiffness as opposed to non-prestressed composite steel beams. Lee et al. (2015) carried out analogous tests to that by Kim and Lee (2011) and reported similar improvements in the performance of PCBs.

In order to supplement experimental works, a number of researchers also advocated the use of analytical and numerical tools to investigate other aspects of structural behavior and performance of PCBs (Hwang et al., 2015; Moscoso et al., 2017; Ng and Tan, 2006b; Ren et al., 2018; Zona et al., 2009). For instance, Ng and Tan (2006b) proposed an analytical approach to evaluate moment capacity of PCBs, as well as to trace load-deflection response and associated stress state in prestressed tendons. The research programs carried out by Dall'Asta and Zona (2005; 2008; 2009) have led to the development of a variety of numerical models that examined the response of PCBs under a combination of loading conditions. Ren et al. (2018) derived another analytical approach to assess flexural behavior of deep composite beams that are externally prestressed using multi-tendon configurations. These researchers proposed a simple technique to evaluate the flexural strength of PCBs that does not require carrying out a nonlinear analysis.

In lieu of simple methods and analytical approaches, few researchers carried out advanced calculation methods (i.e. finite element simulations) to explore the response of PCBs. The pioneering work of Chen and Zhang (2006) and Chen and Jia (2010) was tailored to explore design and detailing aspects of PCBs. These researchers developed highly nonlinear FE models to arrive at optimal effective width as well as to investigate mechanisms of inelastic buckling of PCBs. In their works, Chen and Zhang (2006) noted how the effective width of PCBs could be slightly greater than that of non-prestressed beams. On the other hand, Chen and Jia (2010) reported that buckling resistance of simply supported PCBs is influenced by a collection of factors such as the level of applied loading, slenderness of steel section, and the ratio of span-to-lateral radius of gyration of top flange, among other factors. Another work worthy of mentioning is that carried out by Lou et al. (2016). Lou et al. (2016) created an advanced model to study the behavior of PCBs subjected to short and long-term load duration by incorporating creep effects into their simulations.

As can be seen, the bulk of the published works were primarily designed to examine the performance of isolated PCBs at working (ambient) conditions. In practice, beams are restrained by adjacent members. Such restraints are of complex nature and could limit a beam's ability to laterally or transversely move beam's boundaries (ends) to rotate. In other words, and once put into the field,

This is a preprint draft. The published article can be found at: https://doi.org/10.12989/scs.2021.41.5.625

Please cite this paper as:
Zhou, H., Li, S., Zhang, C., **Naser M.Z.** (2021). "Modeling fire performance of externally prestressed steel–concrete composite beams." *Steel and Composite Structures.* https://doi.org/10.12989/scs.2021.41.5.625

PCBs are expected to have some degree of restraint. This additional restraint adds another level of complexity to PCBs, and may, in fact, change these beams' behavior under certain conditions, most notably fire (Zhou et al., 2018).

Fire is a severe loading condition that subjects a given PCB to the simultaneous effects of heat (thermal loading) and gravity (mechanical) loading (Kodur and Naser, 2014). Heating effects are notorious for degrading the strength and modulus properties of construction materials and hence reducing the overall sectional capacity of PCBs. Given that most PCBs are installed without insulation, the adverse effects of fire are expected to significantly affect the performance of PCBs. It is interesting, and to some degree concerning, to report that there are very limited fire tests carried out to examine the performance of PCBs under fire conditions, with even scare tests to examine the fire performance of restrained PCBs. Up to the authors' knowledge, only two studies investigated fire performance of PCBs and only one of them was carried out on PCBs without corrugated webs (Kang et al., 2016; Zhou et al., 2018). Kang et al. (Kang et al., 2016) studied the effect of the cover thickness of the fire protection material and the shape of corrugated webs on the fire performance prestressed composite beams with corrugated webs. Zhou et al. (Zhou et al., 2018) investigated the fire performance of externally prestressed composite beams with different tendons configurations under different load levels. The limited work in this research area is the main motivation of pursuing this work.

With the hope of narrowing this gap, we showcase the development of a highly nonlinear FE model that is specifically designed to trace thermal and structural response of fire-exposed PCBs. In order to attain a genuine behavior, this model accounts for key factors such as; geometric and material nonlinearities, temperature-dependent material properties, prestressing and bonding effects, as well as traces various failure limit states. The presented model was first developed and validated using fire tests carried out by the authors in a companion work, and then the properly validated FE model was used to examine four primary factors, including effect of restraints (axial vs. rotational), degree of stiffness of restraints, the configuration of external prestressed tendons and magnitude of applied loading, and their effects upon the performance of fire-loaded PCBs.

2.0 Development of the numerical model

This section starts with a description on procedures used in developing the FE model on the PCBs. Then, the FE model is validated against a published test data on a simplified beam at high temperature to demonstrate the validity of the FE model established in this paper.

2.1 Description of finite element models

To this day, the collected literature above shows that most PCBs were tested with simply supported end conditions (see Fig. 1). To investigate the effect of axial and rotational restraints on the fire resistance of PCBs, numerical models including axial and rotational restraints were built. In these models, the axial and rotational restraints were simulated by axial and rotational springs, respectively. These restraining effects on PCBs arising from on-site elements surrounding a PCB (i.e. adjacent columns/beams) were modeled by springs. The stiffness of the axial and rotational springs, α_K and α_r, are critical parameters to investigate (as will be seen in Secs. 3.1 and 4.1). In order to present a realistic view into the fire response of PCBs, the stiffness of restraints will be varied to represent different restraining conditions that could arise in a real fire (i.e. assuming that degradation in members adjacent to PCBs occurs gradually. In the analysis models, each of the analyzed beams will be subjected to two identical concentrated forces located at one-third positions along the span of the beams. These forces are chosen to reflect a pre-defined load ratio varying from 20% to 80%.

This is a preprint draft. The published article can be found at: https://doi.org/10.12989/scs.2021.41.5.625

Please cite this paper as:
Zhou, H., Li, S., Zhang, C., **Naser M.Z.** (2021). "Modeling fire performance of externally prestressed steel–concrete composite beams." *Steel and Composite Structures.* https://doi.org/10.12989/scs.2021.41.5.625

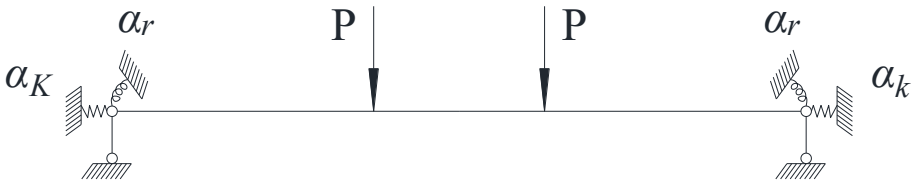

Fig. 1 Incorporating restraining effects to PCBs

In order to simulate fire testing in ABAQUS, a sequentially thermo-mechanical coupled simulation strategy is adopted to investigate the thermal and structural response of the fire-exposed and restrained PCBs. In this coupled approach, the heat transfer analysis was first conducted to obtain temperature distribution within the fire-exposed structures, and then these temperatures are applied to the nodes in structural FE models to account for temperature-induced material degradation in the structural analysis as to obtain deflections, stresses, and failure mechanisms. In the analysis, to conveniently import the nodal temperature to the nodes of the mechanical model, the grid density of the thermal FE model is the same as the mechanical FE model.

In all models, the steel beam is modeled by using shell element DS4 and S4 for heat transfer analysis and mechanical analysis, respectively. In order to reflect the thick nature of the slab as well as the propensity of concrete to crack, the concrete slab was modeled using DC3D8 and C3D8 brick elements for thermal analysis and mechanical analysis, respectively. Both the steel reinforcement (in slab) and external tendons are modeled using link element DC1D2 and T3D2 in heat transfer analysis and mechanical analysis, respectively. The end conditions represented with axial and rotational restraints were also included into the FE model and these were modeled with spring2 elements. The discretized (edge) size of the above-selected elements is 30 mm for shell elements used in steel beam and 20 mm × 40 mm × 30mm for the brick elements used in the concrete slab. These sizes are selected as they pertained to realizing good accuracy with optimum solution time.

In the first stage of analysis, the soffit of the slab was fully tied to the top flange of the beam to eliminate any heat gaps and facilitate the development of thermal gradients normal to this interface. Further, proper heat transfer coefficients were applied as per Eurocode 1 provisions to properly simulate the different heat transfer mechanisms (CEN, 2002). Such coefficients include convection coefficients of 25 w/m.°C, 4 w/m.°C, which were applied at fire exposed surfaces, and unexposed surfaces, respectively, as well as radiation coefficients i.e. Stefan-Boltzman radiation coefficient of 5.669×10^{-8} W/m^2.K^4, and emissivity of 0.7 for both of beam and slab. In the thermal analysis, three sides of the beams, namely, the bottom and the two sides of the cross section were exposed to fire, and the top surface of the concrete slabs were kept at ambient temperature. The air temperature-time curve was ISO834 curve. From the basic assumption above, it is obvious that the temperature distribution along the axis of the beams is uniform.

Similarly, appropriate simulation strategies were also applied to the structural model. For example, the nodes of the elements used to discretize embedded steel reinforcement were tied with those of the concrete slab to ensure compatible deformations. Further, the surface of the upper flange was bonded to the bottom of the slab via contact elements (CONN3D2) along the axis of the beam on the interface. The shear-slip relationship was incorporated by applying Cartesian-Align method to the formulation of CONN3D2. The stiffness of Cartesian-Align needed to ensure this contact was expressed as suggested by Ollgaard et al. (1971) by the following equation:

$$V_T = V_u k_T \left(1 - e^{-\delta}\right)^{0.558}$$

This is a preprint draft. The published article can be found at: https://doi.org/10.12989/scs.2021.41.5.625

Please cite this paper as:
Zhou, H., Li, S., Zhang, C., **Naser M.Z.** (2021). "Modeling fire performance of externally prestressed steel–concrete composite beams." *Steel and Composite Structures.* https://doi.org/10.12989/scs.2021.41.5.625

$$k_T = \begin{cases} 1 & 20 \le T_s < 375 \\ 6.35 \times 10^{-9} {T_s}^3 - 1.341 \times 10^{-5} T_s + 7.382 \times 10^{-3} {T_s}^2 - 0.2168 & 375 \le T_s < 1000 \\ \dfrac{0.5 - T_s}{2400} & 1000 \le T_s < 1200 \end{cases}$$

where, V_T is the shear force at temperature (T_s), k_T is the reduction coefficient, δ is the slip between the concrete slab and the top flange.

The elastic stiffness of the springs was determined according to the distribution and layout of shear studs. The initial prestress in the external tendons was applied by cooling the tendons to target temperatures first, while the other parts of the PCBs were kept under constant temperature. The cooling temperature was determined based on the equivalent strain, namely, the cooling temperature is determined by ensuring that the contraction generated by thermal strain of the external tendons equals that of the prestressing force. As can be seen in Fig. 1, kinematic springs at two ends of the beams were used to model the restraint effects generated from adjacent members. These springs were simulated using two rigid planes, defined at the cross-sections of the two ends in the beam.

The temperature-dependent thermal and mechanical properties of concrete and steel were adopted from Eurocodes 2 and 3 (2004; 2005). It should be noted that structural steel used in the beam was also modeled taking into account strain-hardening effects. The mechanical properties for the external tendons were adopted from actual measurements carried out by Zhou et al. (2008) and the properties for the steel studs were adopted from Chen (2013). In addition, prestress in the cable tension is directly extracted from the result files of numerical models that take into account the effects of temperature expansion, plastic evolution, and coordinated deformation of cables and composite beams.

2.2. Validation of numerical models

Before investigating the behavior of restrained PCBs, the FE models were first validated against PCBs tested under fire and simply supported conditions (Zhou et al., 2018). For this aim, the numerical simulations of the tested data in (Zhou et al., 2018) by using the developed model in this paper are compared with the tested data obtained from the authors' previous fire tests. The experiment in literature (Zhou et al., 2018) is summarized as follows.

Four PCBs named PC-1 to PC-4 were investigated in the literature. The four PCBs consisted of a two-strand prestressed plate-welded steel section attached to a reinforced concrete slab. The first three beams had straight strands, and the fourth beam had draped strands configuration (see Fig. 2). Each beam had a 10 mm thick bottom and top flange. The same flanges had a width of 150 mm. The height and thickness of web in each of these beams were 300 mm and 8 mm, respectively. The PCBs had a full length of 5.3 m with 4.4 m effective span between end supports. Further, each beam was supplemented with bearing stiffeners. These stiffeners were welded at locations supporting applied loading or reaction forces. The stiffeners measured 56 mm (width) × 280 mm (length) × 15 mm (thickness). All beams were made of steel grade Q235 (with a nominal yield strength of 235 MPa). The concrete slab was attached to the beam via two rows of welded 13 mm diameter shear studs. The concrete slab had a rectangular cross-section that measured 800 mm wide and 100 mm thick and was made of Class C35 concrete (as per Chinese code for concrete structures). The steel strands were made of high-strength steel of grade 1862 MPa. These strands were post-tensioned with prestress ratios of 70% for the first, third and fourth beams and 60% for beam PCB-2. These beams were loaded by a hydraulic jack, which applies mechanical loading on the mid-span of a distribution beam, and the distribution beam is supported on the two loading points of the tested specimen. The two

This is a preprint draft. The published article can be found at: https://doi.org/10.12989/scs.2021.41.5.625

Please cite this paper as:
Zhou, H., Li, S., Zhang, C., **Naser M.Z.** (2021). "Modeling fire performance of externally prestressed steel–concrete composite beams." *Steel and Composite Structures.* https://doi.org/10.12989/scs.2021.41.5.625

symmetrically placed point loads have a load ratio of 35% for the first two (PCB-1 and PCB-2) beams and 22% for beams PCB-3 and PCB-4. These loads were kept constant during the test until the critical states of the specimens. These loads were kept constant during the test until the critical states of the specimens. The numerical model for thermal analysis and mechanical analysis, such as element type, material model, and connection between the top concrete slab and top flange of the bottom steel beam, is the same as the model introduced in Sec 2.1. The thermal outcome of the thermal model, namely, nodal temperature, is input as the known condition for the mechanical model.

The four PCBs were subjected to ISO834 fire and failed within 20-30 minutes of fire exposure after reaching a temperature in the range of 740-806°C.

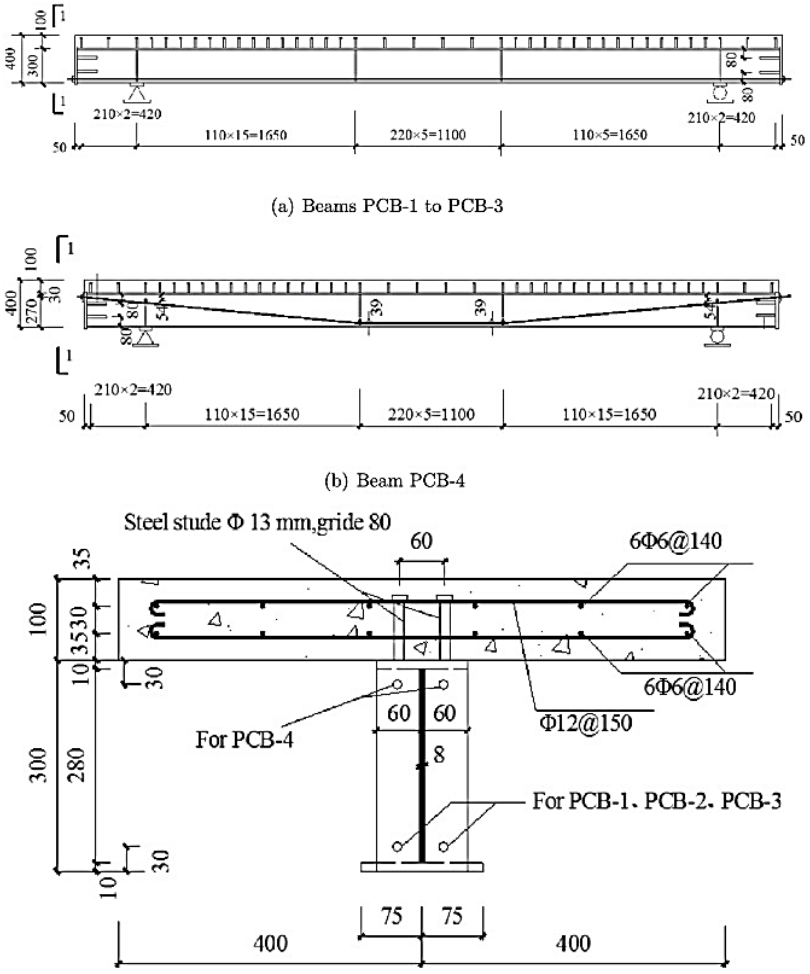

Fig. 2 Geometric details of PCBs (Zhou et al., 2018)

The outcome of this validation is shown for all beams in Fig. 3*. This figure compares numerically

* The thermal validation of these beams was not shown herein for brevity as the thermal response of simply supported and restrained beams is similar. The thermal validation of simply supported beams can be found elsewhere (Zhou et al., 2018).

This is a preprint draft. The published article can be found at: https://doi.org/10.12989/scs.2021.41.5.625

Please cite this paper as:
Zhou, H., Li, S., Zhang, C., **Naser M.Z.** (2021). "Modeling fire performance of externally prestressed steel–concrete composite beams." *Steel and Composite Structures.* https://doi.org/10.12989/scs.2021.41.5.625

predicted and experimentally measured mid-span deflections and transient loss in prestressing force in the external tendons as a function of temperature. It can be seen that the plotted comparisons adequately show the high prediction capabilities of the developed FE models as these results agree well with the test data throughout all stages of analysis. Especially, the tension in the cables tendon agrees with the tested tension in the cable strands, except for PCB-2.This can be attributed to a slight mismatch in the temperature domain in the furnace relative to ISO834. In general, the numerical models in this study can be confidently extended to investigate the behavior of restrained PCBs when subjected to combined effects of fire and external loads.

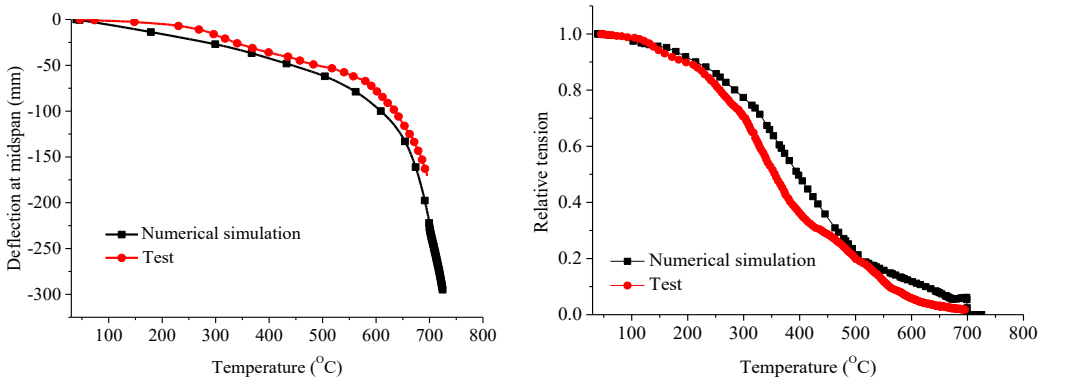

PCB-1

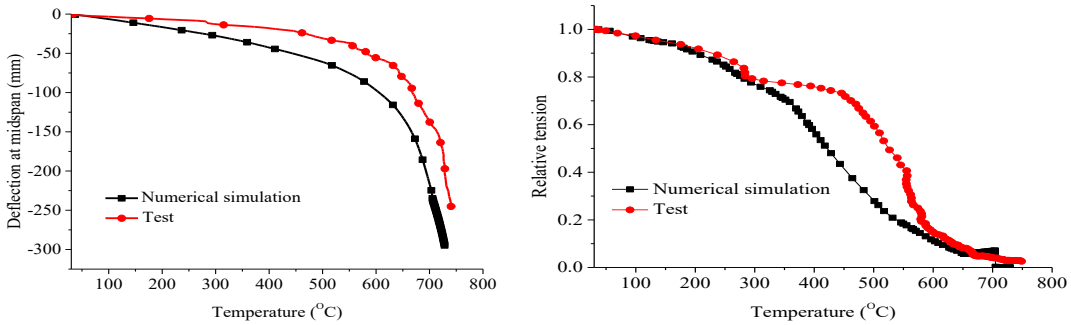

PCB-2

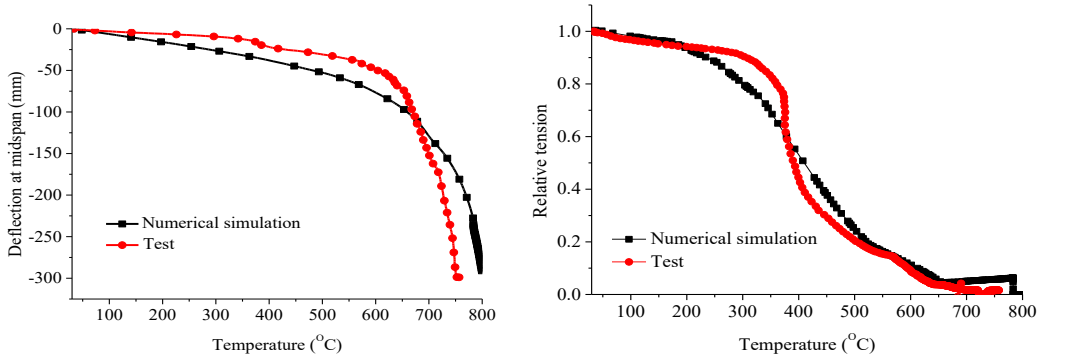

PCB-3

This is a preprint draft. The published article can be found at: https://doi.org/10.12989/scs.2021.41.5.625

Please cite this paper as:
Zhou, H., Li, S., Zhang, C., **Naser M.Z.** (2021). "Modeling fire performance of externally prestressed steel–concrete composite beams." *Steel and Composite Structures.* https://doi.org/10.12989/scs.2021.41.5.625

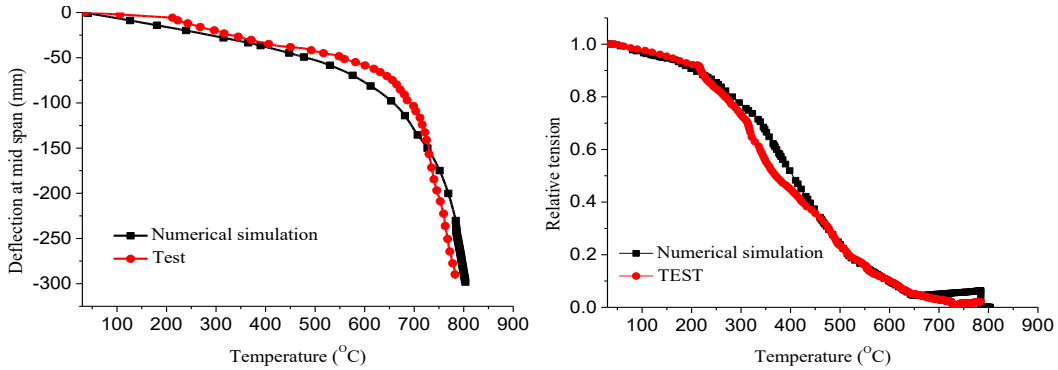

PCB-4

Fig. 3 Comparison of predictions from FE simulations against measurements from fire tests [15] (Left: Mid-span deflection with temperature, Right: Loss of prestress force)

3.0 Parametric study

Now that the FE models are properly validated, these models are applied to explore the effect of axial and rotational restraints, the magnitude of load ratio, as well as prestressing tendon configuration. The specific parameters are shown in Table 1. Discussed in this paper is the structural response under the standard ISO834 curve. Since the beams share a similar configuration and are not insulated, then these beams have similar temperature rise (see Fig. 4). Based on the above assumptions, this paper only plots the structural response of PCB beams in composite beams with temperature as a variable rather than time.

Table 1 Investigated parameters

Paramaters	Variation range
Ratio of axial restraint α_K	0.02, 0.2, 0.5, 1.0
Ratio of load α_F	0.2, 0.4, 0.6, 0.8
External tendon configuration	Bent-up cable; straight cable
Ratio of rotational restrain α_r	0.02, 0.2, 0.5, 1.0

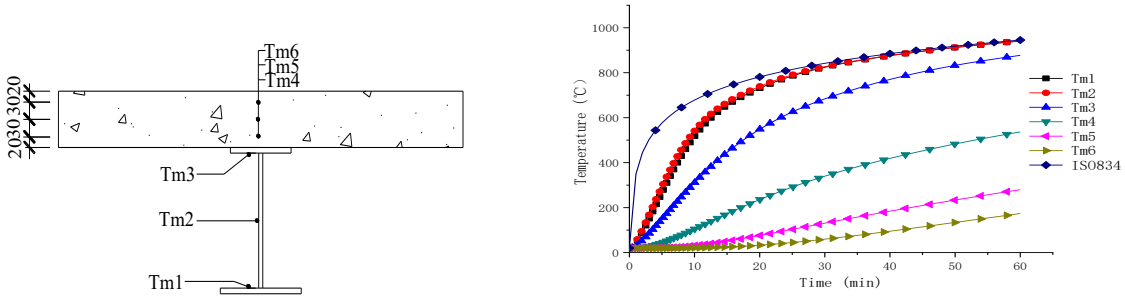

Fig. 4 Simulations of temperature in the cross-section of PCBs

3.1. Examination of axially restrained PCBs

3.1.1. Effect of axial restraint

Figure 5 displays the resulting mid-span deflection, axial force, ratio of prestress loss in the external tendons and secondary moment for the PCB beam with bent-up cable for load ratio (α_F) 40% and various

This is a preprint draft. The published article can be found at: https://doi.org/10.12989/scs.2021.41.5.625

Please cite this paper as:
Zhou, H., Li, S., Zhang, C., **Naser M.Z.** (2021). "Modeling fire performance of externally prestressed steel–concrete composite beams." *Steel and Composite Structures.* https://doi.org/10.12989/scs.2021.41.5.625

levels of axial restraints (of 0.02, 0.2, 0.5 and 1). Here, the secondary moment is defined as *p-δ* effect. Namely, the moment is obtained by multiplying the deflection at mid-span and the axial force in the beam. This figure shows how the behavior of the restrained PCBs can be grouped under five stages (I-V). The five stages are grouped according to the evolution of the slope of axial force curves in the beams (see Fig. 5b). At stage I, the axial force reaches its maximum compression force, and at the end of stage II, the axial force decrease. At the end of stage III, the axial force reaches zero. In stages IV and V, the axial force becomes tension force. Taking $\alpha_K = 0.5$ as an example, the first stage (occurring between 20°C to 390°C) witnessed how the mid-span deflection increases in a slow and linear fashion (refer to Fig.5a), despite the fact that degradation in mechanical properties were negligible. This rise in deformation was triggered by thermal bowing effects resulting from generated temperature gradient through the cross-section. For the same case, the amount of negative axial force increases steadily (Fig.5b), prestressing force decreases (Fig.5c), and the sagging secondary moment increases (Fig.5d). This increase in the amount of the restrained axial force and the accompanying decrease in the prestressing force were mainly caused by fire-induced thermal strains.

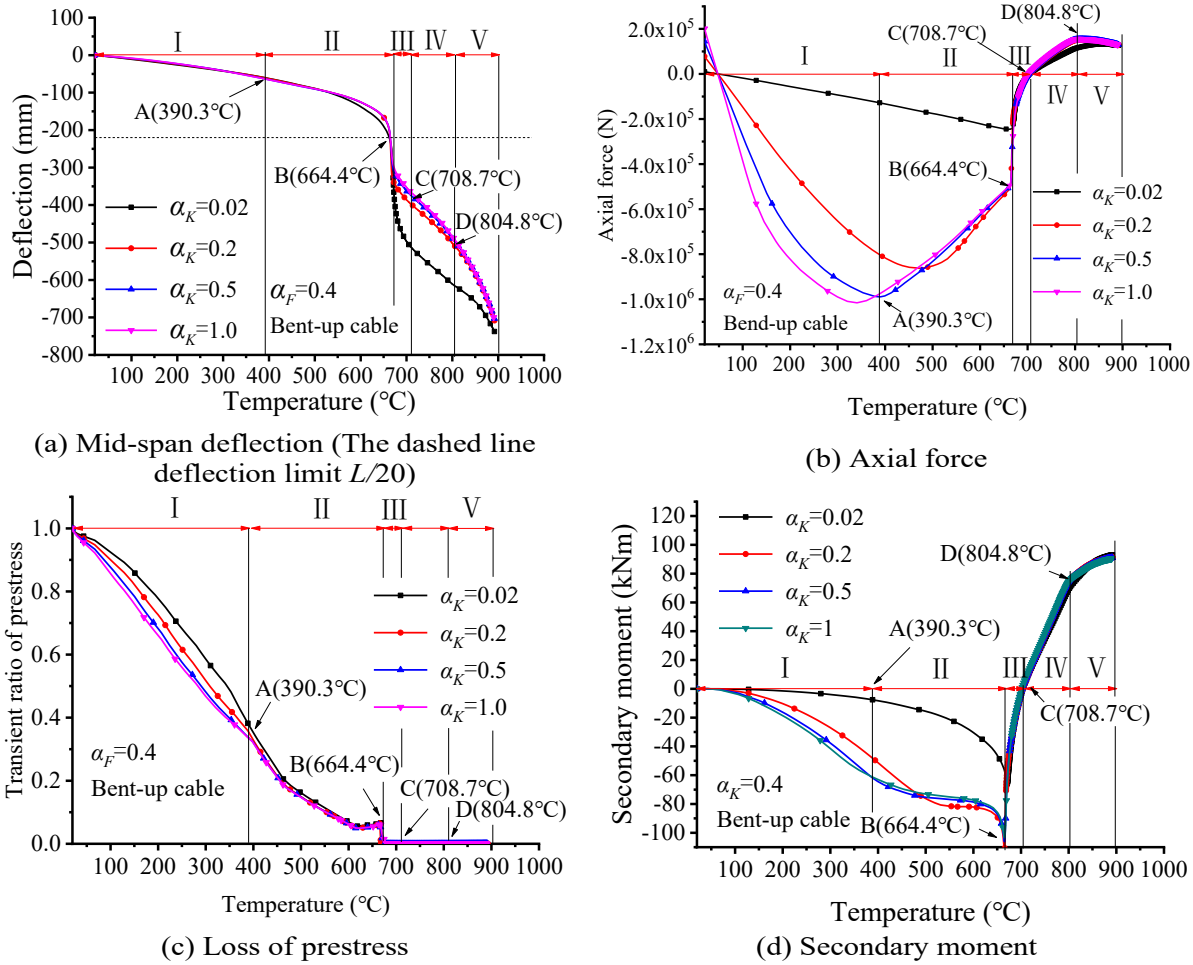

(a) Mid-span deflection (The dashed line deflection limit *L*/20)

(b) Axial force

(c) Loss of prestress

(d) Secondary moment

Fig. 5 Effect of axial restraint on the fire resistance of PCBs (temperatures were measured at the bottom flange of the steel section)†

† Please note that the axial force was taken as the reaction force at the axial restraint connected to the beam end (-ve: compression state and +ve: tension state); The secondary moment was the moment caused by the P-delta effect (-ve: sagging, +ve: hogging); α_k and α_r were calculated as the ratio of the stiffness of the axial or rotational restraint to the

This is a preprint draft. The published article can be found at: https://doi.org/10.12989/scs.2021.41.5.625

Please cite this paper as:
Zhou, H., Li, S., Zhang, C., **Naser M.Z.** (2021). "Modeling fire performance of externally prestressed steel–concrete composite beams." *Steel and Composite Structures.* https://doi.org/10.12989/scs.2021.41.5.625

At stage II, from 390°C to 664°C, the mid-span deflection and sagging secondary moment continue to increase at a quicker pace, while the amount of the negative axial force decreases, and prestress loss continues to decrease. In this stage, the mechanical properties of steel and concrete significantly reduce, and, in response, the amount of the axial force also decreases (Fig. 5b). The prestressing forces in tendons drop at a slightly high rate due to the combined effects of material deterioration and rise in thermal strains. Following this stage is stage III (from 664°C to 709°C). In this stage, the deflection suddenly increases, the prestressing force drops to zero, and as such, both the axial force and secondary moment also drop abruptly. It is in this stage that the bottom flange seems to buckle due to the compressive component of the large hogging moment present at the two ends. At stage IV, from 709°C to 805°C, catenary action activates as the deflection increases, the amount of the positive axial force and hogging secondary moment increase, and the external tendons became fully slacked. At stage V, with temperatures exceeding 805°C, the restrained PCB undergoes large deflection and the axial force cross to the positive region, indicating a tensional state in PCBs.

A closer look into Figs. 5a and 5c show that stiffness of the axial restraint has a negligible effect on the deflection behavior, as well as prestress loss of the restrained PCB at the first two stages (and before the external tendons slack). However, at later stages (III to V or after the external tendons slack and become obsolete), the predicted deflections for the cases with axial restraint stiffness ($\alpha_K \geq 0.2$) were similar and also greater than the case with small axial restraint stiffness ($\alpha_K = 0.02$). It is apparent that the use of weak axial restraints does not seem to fully utilize catenary action and lead to premature failure. On the other hand, Figs. 5b and 5d show that the stiffness of the axial restraint has a much prominent effect on the predicted axial force and the secondary moment before the external tendons slack, but this effect seems to become minor at the later heating stages/after tendons slack.

Failure can be defined following thermal or mechanical criteria. In our tests, we relied on the mechanical criterion in which a beam is "declared" to fail once its deflection exceeds the L/20 limit. However, this limit is an artificial limit applied to protect fire furnaces from failure (i.e., it is observed that when beams deflect to a large extent, this deflection can runaway and break the testing equipment. In reality, the L/20 limit does not always coincide with the strength limit state (i.e., failure occurring once the moment or shear capacity is exceeded), but rather by a serviceability limit.It is interesting to note that under a standard fire testing regime, failure of beams occurs once mid-span deflection exceeds a deflection limit *L/20* (where, L = supporting length). By applying this criterion and through examining Fig. 5a, it is clear that all of these beams fail at the same temperature of 660°C despite having different axial restraints. This temperature also corresponds to the same point in time when external tendons lose all prestressing force and slack. In our tests, the tested specimens were subjected to tension prestressing, and these beams also have a large reserve (under and flexure moment) that we noticed to be activated (e.g., enable beams to continue to carry the applied loading even once L/20 criterion is exceeded). Fig. 5 shows that these beams with catenary effect have great fire resistance even when the deflection exceeds L/20. Therefore, this paper did not use the artificial L/20 as the criterion of critical states of the composite beams with axial restraints, but rather we used our real observations.

3.1.2. Effect of load ratio

The above developed FE model for the case of a PCB with bent-up tendons was also used to investigate the effect of load magnitude (α_F ratio). The outcome of this analysis is plotted in Fig. 6 for the case of axial stiffness ratio (α_K) of 1.0. These plotted results clearly illustrate how applied load ratio has a substantial

axial or bending stiffness of the composite beam without external tendons, at ambient temperature.

This is a preprint draft. The published article can be found at: https://doi.org/10.12989/scs.2021.41.5.625

Please cite this paper as:
Zhou, H., Li, S., Zhang, C., **Naser M.Z.** (2021). "Modeling fire performance of externally prestressed steel–concrete composite beams." *Steel and Composite Structures.* https://doi.org/10.12989/scs.2021.41.5.625

influence upon the predicted response of PCBs in terms of deflection, development of axial force, and secondary moment. Overall, one can deduce that higher load levels lead to a lower temperature at failure‡ (implying early failure times). For example, the failure temperature was 776°C for α_F = 0.2 and 519°C for α_F = 0.8, representing load ratios of 20% and 80%, respectively. Figure 6b and 6c show how that the predicted axial force (up to 500°C) and loss in prestressing force are not sensitive to the magnitude of load ratio before buckling. On the other hand, Fig. 6d shows that the load ratio has a significant effect on the predicted secondary moment. It is worth reminding the reader that beyond 500°C, the axial force was mainly governed by temperature level and stiffness of the axial restraint, while the prestressing force was mainly determined by the thermal strain.

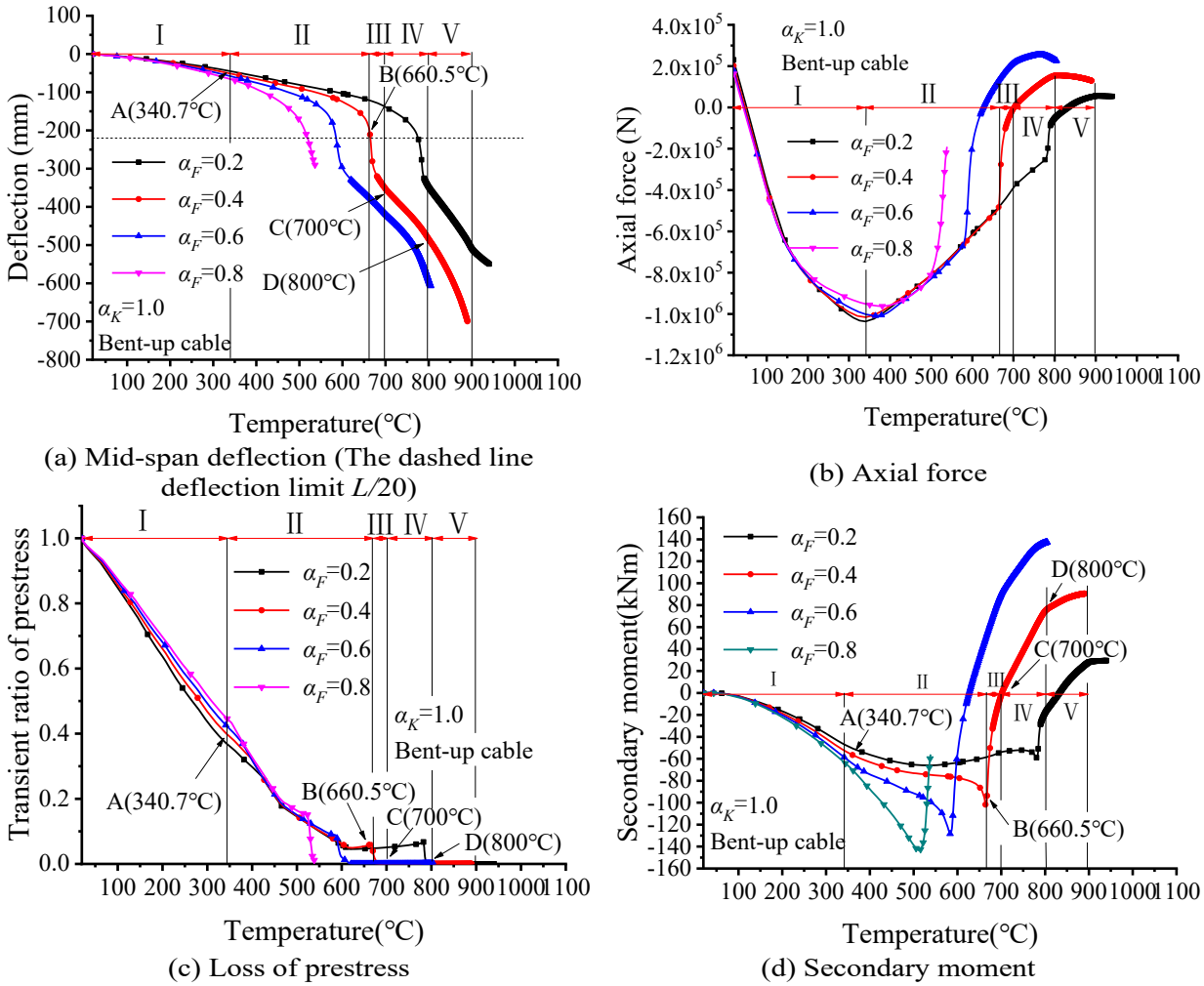

(a) Mid-span deflection (The dashed line deflection limit *L*/20)

(b) Axial force

(c) Loss of prestress

(d) Secondary moment

Fig. 6 Effect of load ratio on the fire resistance of PCBs with axial restraints (α_K = 1.0)

3.1.3. Effect of external tendon configuration

Figure 7 compares the predicted behavior in PCBs with two different external tendon configurations (bent-up and straight cable) for a load ratio α_F = 0.4 and 0.2, 0.5 and 1.0 of axial restraint ratio. Fig. 7a shows the beams with straight cable strands and lower axial restraint, 0.2 and 0.5 of restraint ratio, have

‡ Failure was defined according to the deflection criteria (i.e. *L/20*) (ASTM, 2016). This criterion is used throughout this study.

This is a preprint draft. The published article can be found at: https://doi.org/10.12989/scs.2021.41.5.625

Please cite this paper as:
Zhou, H., Li, S., Zhang, C., **Naser M.Z.** (2021). "Modeling fire performance of externally prestressed steel–concrete composite beams." *Steel and Composite Structures.* https://doi.org/10.12989/scs.2021.41.5.625

less deflection at the critical stage than those with 1.0 of axial restraint ratio. This can be explained from Fig. 7 b, which shows that the tension is greater in the straight cable of the beam with 0.2 and 0.5 of restraint ratio than that with 1.0 of axial restraint ratio, especially in the stage I, II. Consequently, these greater tension the cable strands produce great hogging moment, which make the deflection of the beams with straight cable strands develop slowly.

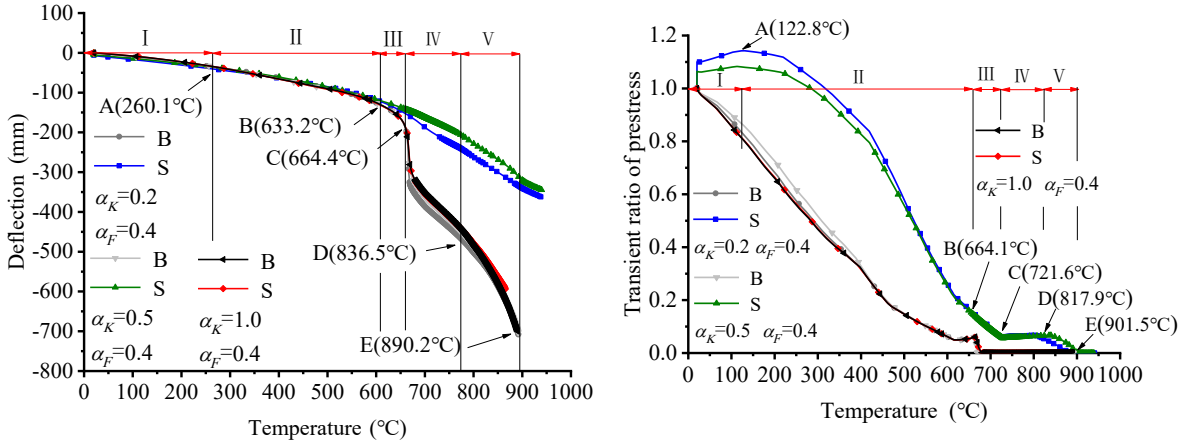

(a) Mid-span deflection (The dashed line deflection limit *L*/20)

(b) Loss of prestress

Note: in the Fig B denotes Bent-up cable, C denotes Straight cable

Fig. 7 Effect of tendon configuration on the fire resistance of PCBs with axial restraints ($\alpha_F = 0.4$)

3.2. Examination of axially and rotationally restrained PCBs

Once the above analyses were completed, the developed models were modified to incorporate both axial and rotational restraints. The outcome of this analysis is presented herein.

3.2.1. Effect of rotational restraint

Figure 8 shows the results of mid-span deflection, axial force, loss in prestressing force in external tendons, as well as secondary moment for the PCB of bent-up tendon configuration (with load ratio α_F = 0.4, and axial restraint ratio α_K = 1.0) as a function of fire exposure temperature and various rotational restraints. This figure illustrates that when the rotational restraint was weak (α_r = 0.02), the deflection of the PCB had a sudden drop at 680.4°C, similar to that of the PCB with weak axial restraint (compare Fig. 8a to Fig. 5a where a similar drop occurred at 664.4°C). This indicates the negligible effect of weak rotational restraints. On the other hand, when the rotational restraint was high ($\alpha_r \geq 0.2$), the predicted deflections did not undergo a similar behavior to that observed in the case of weak restraint nor to that in the case with axial restraints only; possibly due to the fact that the additional rotational flexibility negated buckling of bottom flange (see Fig. 5a). The difference between Figs. 8a and 5a highlight the positive effects of combining rotational and axial restraints, which seem to improve deflection response and extend failure of PCBs beyond that where only axial restraints are incorporated.

This is a preprint draft. The published article can be found at: https://doi.org/10.12989/scs.2021.41.5.625

Please cite this paper as:
Zhou, H., Li, S., Zhang, C., **Naser M.Z.** (2021). "Modeling fire performance of externally prestressed steel–concrete composite beams." *Steel and Composite Structures.* https://doi.org/10.12989/scs.2021.41.5.625

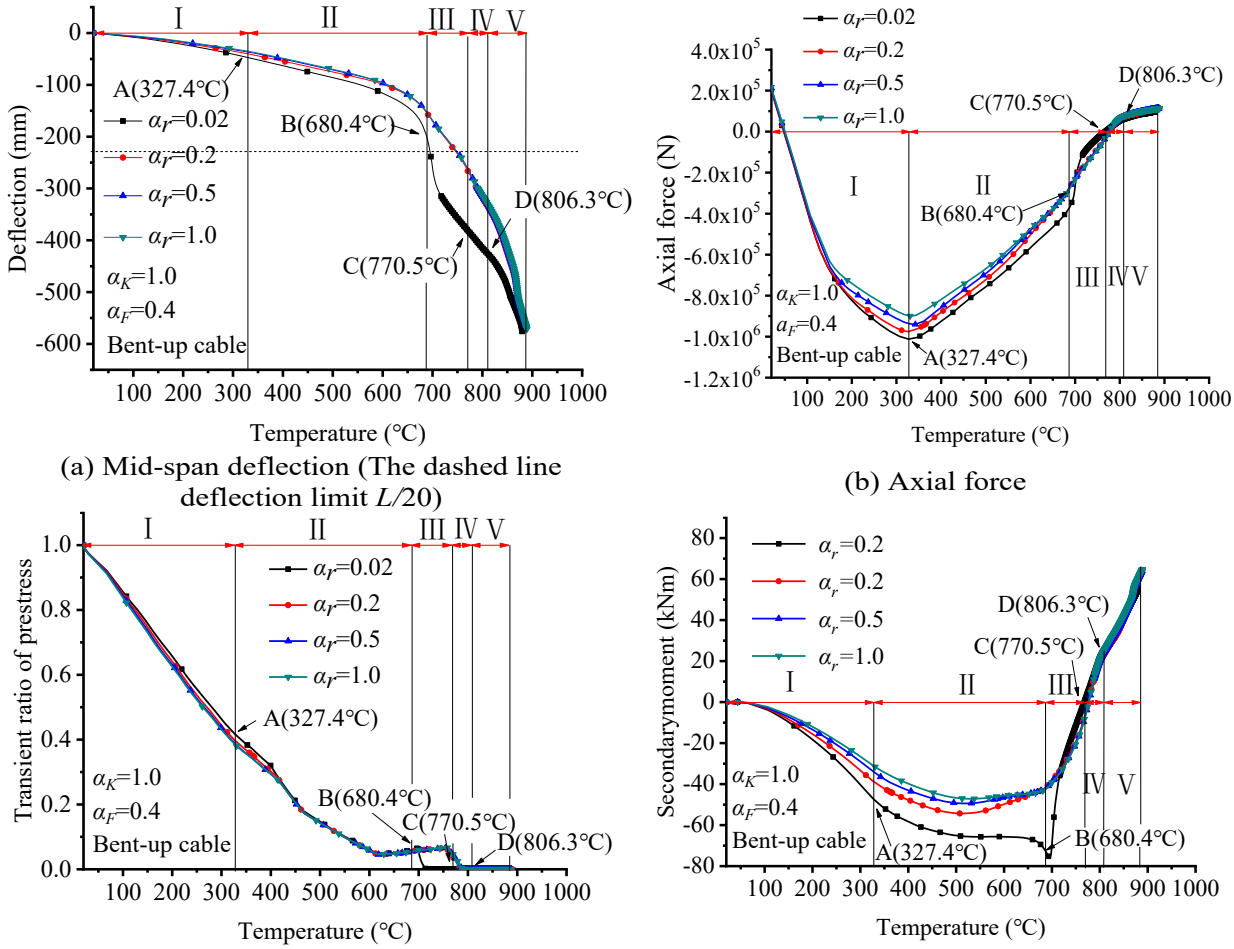

Fig. 8 Effect of rotational restraint ratio on the fire resistance of PCBs with axial and rotational restraints (α_K = 1.0)

Further, stiffer PCBs were able to develop high axial forces as a result of sustaining end moments. Under nearly the same deflection (Fig 8a), the axial force of PCBs with a smaller ratio of rotational stiffness are larger than that of PCBs with larger ratios of rotational stiffness (Fig. 8b). As in other cases, the stiffness of the rotational restraints had a negligible effect on the prestressing force (Fig. 8c). Using the failure criteria in the standard fire test, the failure temperature was 693°C for the beam with the weak rotational restraint (α_r = 0.02) and 742°C for beams with strong rotational restraints ($\alpha_r \geq 0.2$). While the difference in failure temperature between these two beams is about 50°C, this still highlights the positive effects of rotational restraints of 0.2, 0.5 and 1.0.

3.2.2. Effect of load ratio

Figure 9 shows the predicted behaviors for the PCBs with bend-up tendons, axial restraint ratio of 1.0, and rotational restraint ratio of 1.0 for various magnitudes of load levels. Similar to the findings presented in Sec. 3.1.2, the load ratio also seems to have a measurable effect on the deflection behavior of PCBs (i.e. the higher the load ratio, the larger the deflection). This is due to the additional stresses generated from the higher level of loading, and when this is combined to the severe degradation in properties of constituent materials at high temperature, this results in a drop in flexural stiffness; thus, promoting higher deflections. The failure temperature in two representative beams is estimated at 850°C for α_F = 0.2 and 650°C for α_F =

This is a preprint draft. The published article can be found at: https://doi.org/10.12989/scs.2021.41.5.625

Please cite this paper as:
Zhou, H., Li, S., Zhang, C., **Naser M.Z.** (2021). "Modeling fire performance of externally prestressed steel–concrete composite beams." *Steel and Composite Structures.* https://doi.org/10.12989/scs.2021.41.5.625

0.8. Figures 9b and 9d show that, at the early heating stage (below 330°C), the predicted axial force and secondary moment are not sensitive to the value of load ratio.

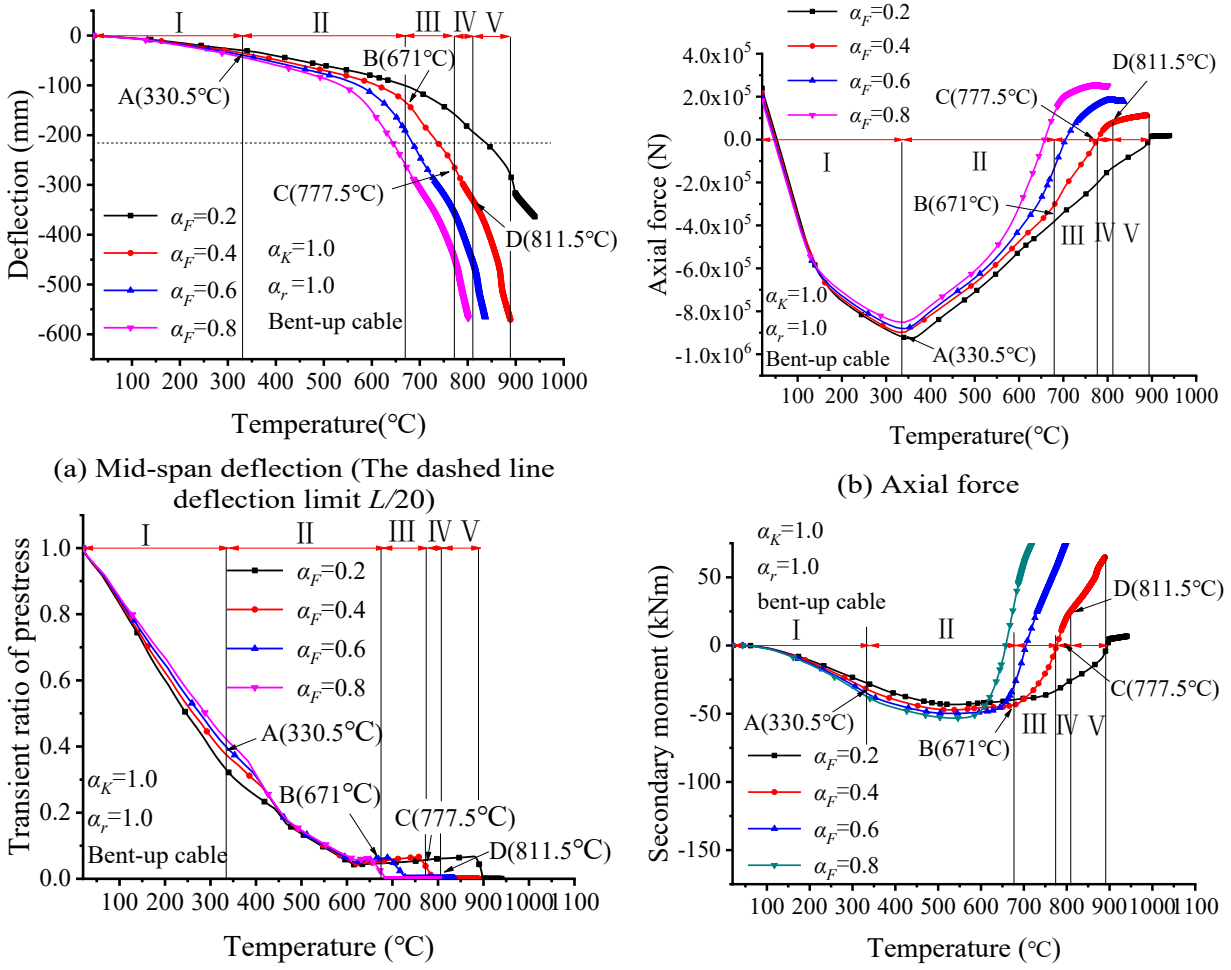

(a) Mid-span deflection (The dashed line deflection limit *L*/20)

(b) Axial force

(c) Loss of prestress force

(d) Secondary moment

Fig. 9 Effect of load ratio on the fire resistance of PCBs with axial and rotational restraints (α_K = 1.0 and α_r = 1.0)

3.2.3. Effect of external tendon configuration

Figure 10 compares the predicted behavior of two identical PCBs (with load ratio α_F = 0.4, the axial restraint ratio α_K = 0.2,0.5,1.0, and the rotational restraint ratio α_r =1.0) but having two different external tendon configurations. This comparison predicts similar deflection and prestressing force in both of the studied beams. Fig. 10a shows beams with 0.2 and 0.5 of α_K have smaller deflection and slightly higher critical temperature in the critical state than those with 1.0 of α_K. This is due to the fact that straight cable strands produce greater tension in the initial stage than the bent-up cable strands due to the larger deformation. This can be validated from the variation of tension in the cable strands in the stage I and II in Fig. 10b, in which the relative tension in the beam with straight cable rise slightly, especially in the stage I. On the other hand, the smaller axial restraint ratio can produce smaller secondary hogging moment, which makes the final deflection smaller at the critical stage and higher critical temperature.

This is a preprint draft. The published article can be found at: https://doi.org/10.12989/scs.2021.41.5.625

Please cite this paper as:
Zhou, H., Li, S., Zhang, C., **Naser M.Z.** (2021). "Modeling fire performance of externally prestressed steel–concrete composite beams." *Steel and Composite Structures.* https://doi.org/10.12989/scs.2021.41.5.625

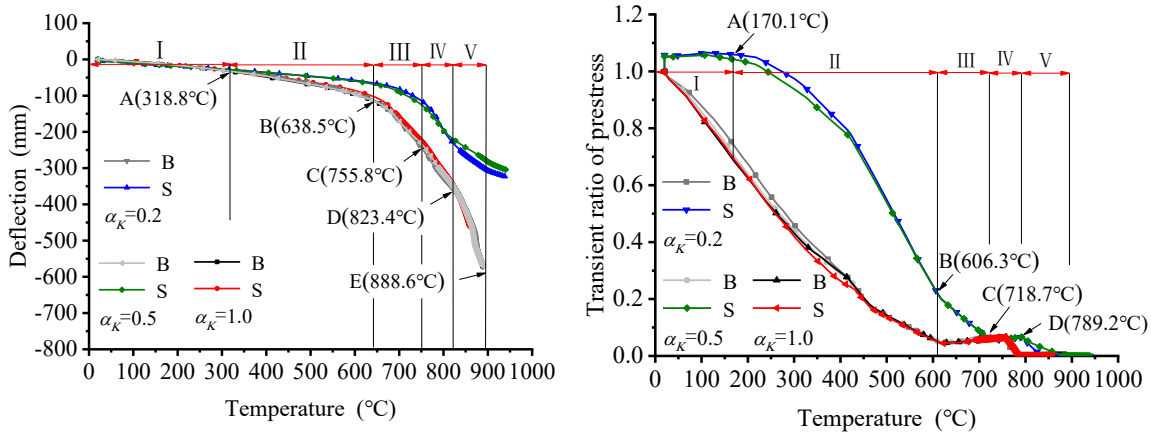

(a) Mid-span deflection (The dashed line deflection limit *L*/20)

(b) Loss of prestress force

Note: in the Fig, "B" denotes *Bent-up cable*, "C" denotes *Straight cable*

Fig. 10 Effect of tendon configuration on the fire resistance of PCBs with axial and rotational restraints (α_F = 0.4 and α_r = 1.0)

4.0 Conclusions

This paper presents a numerical study on the fire response of restrained and prestressed composite beams (PCBs). The main parameters investigated herein are the effect of restraints (axial vs. rotational), degree of stiffness of restraints, configuration of external prestressed tendons and magnitude of applied loading. Based on the analysis carried out herein, the following conclusions can be drawn:

- The effect of load ratio on prestressed composite beam has two sides. On the one hand, when the load ratio is 0.8, the catenary effect is not easily triggered in prestressed steel-concrete composite beams. On the other hand, when the load ratio is 0.2-0.6, catenary effect can be formed. Within this load ratio range, the lower the load ratio, the higher the temperature entering the catenary stage.
- The FE simulations confirm that external tendons slack, leading to failure in a PCB. The slacking of the external tendons could then be used as an indicator of the failure of the restrained PCBs.
- The stiffness of the axial restraint had a minor influence on the failure temperature. On the other hand, the stiffness of rotational restraints was only important in beams with low rotational stiffness.
- The configuration of the external tendon had minor influence on the failure temperature of the externally prestressed composite beams. When the axial restraint ratio does not exceed 0.5, the critical deflection of the composite beam is lower than that of the composite beam with a restraint ratio of 1.0.

5.0 Acknowledgement

The work reported in this paper is partially supported by the National Science Foundation of China under through contract 51878528, 51508399. The support is gratefully acknowledged.

References

ASTM, (2016). "E119-16 - Standard Test Methods for Fire Tests of Building Construction and Materials", *American Society for Testing and Materials*. DOI: 10.1520/E0119-10B.1.2

BSI, and European Committee for Standardization, (2004). *Design of concrete structures - Part 1-2: General rules - Structural fire design*, *Eurocode 2*. DOI: 10.1002/jcp.25002

CEN, (2002). *Eurocode 1: Actions on Structures–Part 1–2: General Actions–Actions on Structures Exposed to Fire*.

This is a preprint draft. The published article can be found at: https://doi.org/10.12989/scs.2021.41.5.625

Please cite this paper as:
Zhou, H., Li, S., Zhang, C., **Naser M.Z.** (2021). "Modeling fire performance of externally prestressed steel–concrete composite beams." *Steel and Composite Structures.* https://doi.org/10.12989/scs.2021.41.5.625

Chen, L., Li, G., Jiang, S., and Wang, W., (2013). "Experimental studies on behavior of headed stud shear connectors at elevated temperatures", *Tongji Daxue Xuebao/Journal of Tongji University*. DOI: 10.3969/j.issn.0253-374x.2013.08.006

Chen, S., (2005). "Experimental study of prestressed steel-concrete composite beams with external tendons for negative moments", *Journal of Constructional Steel Research*. DOI: 10.1016/j.jcsr.2005.05.005

Chen, S., and Jia, Y., (2010). "Numerical investigation of inelastic buckling of steel-concrete composite beams prestressed with external tendons", *Thin-Walled Structures*. DOI: 10.1016/j.tws.2009.10.009

Chen, S., Wang, X., and Jia, Y., (2009). "A comparative study of continuous steel-concrete composite beams prestressed with external tendons: Experimental investigation", *Journal of Constructional Steel Research*. DOI: 10.1016/j.jcsr.2009.03.005

Chen, S., and Zhang, Z., (2006). "Effective width of a concrete slab in steel-concrete composite beams prestressed with external tendons", *Journal of Constructional Steel Research*. DOI: 10.1016/j.jcsr.2005.08.009

Dall'Asta, A., Dezi, L., and Leoni, G., (2002). "Failure mechanisms of externally prestressed composite beams with partial shear connection", *Steel and Composite Structures*. DOI: 10.12989/scs.2002.2.5.315

Dall'Asta, A., and Zona, A., (2005). "Finite element model for externally prestressed composite beams with deformable connection", *Journal of Structural Engineering*. DOI: 10.1061/(ASCE)0733-9445(2005)131:5(706)

Deretic-Stojanovic, B., and Kostic, S. M., (2017). "A simplified matrix stiffness method for analysis of composite and prestressed beams", *Steel and Composite Structures*. DOI: 10.12989/scs.2017.24.1.053

ECS, (2005). *EN 1993-1-2: Eurocode 3: Design of steel structures - Part 1-2: General rules - Structural fire design : European Committee for Standardisation : Free Download, Borrow, and Streaming : Internet Archive*, *European Committee for Standardisation*.

Hoadley, P. G., (1963). "Behavior of prestressed composite steel beams", *Journal of Structural Division*, **89**(3), 21–34.

Hwang, J. W., Kwak, J. H., and Kwak, H. G., (2015). "Finite-Element Model to Evaluate Nonlinear Behavior of Posttensioned Composite Beams with Partial Shear Connection", *Journal of Structural Engineering (United States)*. DOI: 10.1061/(ASCE)ST.1943-541X.0001174

Kang, H., Lee, D. H., Hwang, J. H., Oh, J. Y., Kim, K. S., and Kim, H. Y., (2016). "Structural Performance of Prestressed Composite Members with Corrugated Webs Exposed to Fire", *Fire Technology*. DOI: 10.1007/s10694-015-0521-y

Kim, K. S., and Lee, D. H., (2011). "Flexural behavior of prestressed composite beams with corrugated web: Part II. Experiment and verification", *Composites Part B: Engineering*. DOI: 10.1016/j.compositesb.2011.04.019

Kodur, V. K. R., and Naser, M. Z., (2014). "Effect of shear on fire response of steel beams", *Journal of Constructional Steel Research*, **97**, 48–58. DOI: 10.1016/j.jcsr.2014.01.018

Lee, D. H., Oh, J. Y., Kang, H., Kim, K. S., Kim, H. J., and Kim, H. Y., (2015). "Structural performance of prestressed composite girders with corrugated steel plate webs", *Journal of Constructional Steel Research*. DOI: 10.1016/j.jcsr.2014.09.014

Lorenc, W., and Kubica, E., (2006). "Behavior of composite beams prestressed with external tendons: Experimental study", *Journal of Constructional Steel Research*. DOI: 10.1016/j.jcsr.2006.01.007

Lou, T., Lopes, S. M. R., and Lopes, A. V., (2016). "Numerical modeling of externally prestressed steel-concrete composite beams", *Journal of Constructional Steel Research*. DOI: 10.1016/j.jcsr.2016.02.008

Moscoso, A. M., Tamayo, J. L. P., and Morsch, I. B., (2017). "Numerical simulation of external pre-stressed steel-concrete composite beams", *Computers and Concrete*. DOI: 10.12989/cac.2017.19.2.191

Ng, C. K., and Tan, K. H., (2006a). "Flexural behaviour of externally prestressed beams. Part II: Experimental investigation", *Engineering Structures*. DOI: 10.1016/j.engstruct.2005.09.016

Ng, C. K., and Tan, K. H., (2006b). "Flexural behaviour of externally prestressed beams. Part I: Analytical model", *Engineering Structures*. DOI: 10.1016/j.engstruct.2005.09.015

Ollgaard, J. G., Slutter, R. G., and Fisher, J. W., (1971). "Shear Strength of Stud Connectors in Lightweight and Normal-Weight Concrete", *AISC Engineering Journal*.

Ren, Y., Wang, Y., Wang, B., Ban, H., Song, J., and Su, G., (2018). "Flexural behavior of steel deep beams prestressed with externally unbonded straight multi-tendons", *Thin-Walled Structures*. DOI: 10.1016/j.tws.2018.07.022

Szilard, R., (1959). "Design of Prestressed Composite Steel Structures", *Journal of the Structural Division*, **85**(9),

This is a preprint draft. The published article can be found at: https://doi.org/10.12989/scs.2021.41.5.625

Please cite this paper as:
Zhou, H., Li, S., Zhang, C., **Naser M.Z.** (2021). "Modeling fire performance of externally prestressed steel–concrete composite beams." *Steel and Composite Structures.* https://doi.org/10.12989/scs.2021.41.5.625

97–124.
Zhou, H.-T., Li, G.-Q., and Jiang, S.-C., (2008). "Experimental studies on the properties of steel strand at elevated temperatures", *Sichuan Daxue Xuebao (Gongcheng Kexue Ban)/Journal of Sichuan University (Engineering Science Edition)*.
Zhou, H., Li, S., Chen, L., and Zhang, C., (2018). "Fire tests on composite steel-concrete beams prestressed with external tendons", *Journal of Constructional Steel Research*, **143**, 62–71. Elsevier. DOI: 10.1016/j.jcsr.2017.12.008
Zona, A., Ragni, L., and Dall'Asta, A., (2008). "Finite element formulation for geometric and material nonlinear analysis of beams prestressed with external slipping tendons", *Finite Elements in Analysis and Design*. DOI: 10.1016/j.finel.2008.06.005
Zona, A., Ragni, L., and Dall'Asta, A., (2009). "Simplified method for the analysis of externally prestressed steel-concrete composite beams", *Journal of Constructional Steel Research*. DOI: 10.1016/j.jcsr.2008.07.015